

1 The format of this reply to Referee 1 is as follows:

2

3 In the first part, "**Authors' Response to Anonymous Referee 1**", we  
4 provide a point-by-point response to the referee's comments. We provide each of the  
5 referee's comments in **bold font**. After each comment that requires a response we  
6 provide a response (in regular font). If we modified the manuscript in response to a  
7 comment, we describe what the modification was, and indicate where it was made in the  
8 revised manuscript (the revised manuscript is provided at the end of this document).

9

10 In the second section, **Additional modifications to the manuscript**, we  
11 describe modifications to the manuscript not made in response to any specific comment  
12 of either referee. For the most part these modifications are minor, however we did fix  
13 two errors in the final analytical solution (errors in the text, not the code; so these did  
14 not affect any of the presented results).

15

16 In the third section, we provide the revised manuscript.

17

18 Authors' Response to Anonymous Referee 1

19

20 The authors derive an analytical solution of the two-dimensional steady Boussinesq  
21 equations in the limit of zero Reynolds number. To obtain this solution they transform the  
22 equations into a sixth-order equation for the streamfunction. Then they seek a solution in  
23 the form of a single-harmonic,  $A(z)\cos(kx)$ . Then the general solution is found as an infinite  
24 summation of single-harmonic solutions. The procedure is rigorous and well-described. In  
25 the second part of the paper the authors proceed to use this analytical solutions to test  
26 different boundary conditions for the pressure Poisson equation in a particular numerical  
27 implementation. They consider two cases in which they compare numerical results for  
28 homogeneous and inhomogeneous types boundary conditions for the pressure Poisson  
29 equation to the analytical solution. Only the inhomogeneous boundary condition passes  
30 both tests. In summary, this is an interesting paper that deserves publication. I have several  
31 minor comments:

32

33 **1. Section 2.1: Please explain the physical meaning of equation (3), i.e. that the equation for**  
34 **b is based on the transport equation for the temperature.**

35 Equation (2.3) is the thermal energy equation (differential form of the first law of  
36 thermodynamics). In the revised manuscript we now briefly discuss the governing equations,  
37 including (2.3) in the paragraph right after (2.4). We also give a reference to where the equations  
38 are described more fully (Chandrasekhar 1961). Further down in the paragraph we give a  
39 reference (Kundu 1990) for the Brunt-Väisälä frequency  $N$ , a parameter that appears in (2.3).

40

41 **2. Please specify which condition has been substituted in which equation in order to obtain**  
42 **Eqs. (24-25).**

43 Right before (2.24) we now state that: "In view of (2.7) and (2.17), the impermeability  
44 condition  $w(x,0) = 0$  and no-slip condition  $u(x,0) = 0$  yield"

45

46 **3. Section 2.3: "The derivation of the u field requires considerable effort and is not**  
47 **pursued." I do not understand this. As far as I understand, the analytical solution of u is**

48 **simply the analytical partial derivative of Eq. (39) with respect to  $x$ , which can be explicitly**  
49 **written as an infinite sum. Do I miss anything?**

50 The referee is not quite right. As can be seen from (7), one gets  $u$  by differentiating the  
51 streamfunction (specified in (39)) with respect to  $z$ , not  $x$  [One gets  $w$  by differentiating the  
52 streamfunction with respect to  $x$ , and that's a relatively easy calculation]. Moreover, as can be  
53 seen from (31),  $z$  is implicitly inside four of the factors in (39). This is why obtaining  $u$  is  
54 potentially complicated.

55 However, we decided to go ahead and take the  $z$ -derivative of (39) and see if we could  
56 obtain a relatively compact final form for  $u$ . It turns out that by making use of addition formulas  
57 for sines, the results do simplify considerably and the final form of  $u$  is not too bad. So, we now  
58 present the analytical solution for  $u$ : (2.32) for the single-harmonic wave and (2.41) for the  
59 square wave. The differences between the analytical  $u$  and the  $u$  obtained by finite differencing  
60 the streamfunction are visually imperceptible for tests A-1 and A-2. The quantitative changes are  
61 generally less than 1 % but are on the order of 1 % near the surface. Our reported values for the  
62  $R$  ratios do not change for A-1 but there is a minor change in one of the  $R$  ratios for A-2:  $R_b$  was  
63 originally  $R_b \cong 3.6 \times 10^{-3}$  but is now  $R_b \cong 3.8 \times 10^{-3}$ . The refined value is given in the revised  
64 manuscript. With the analytical solution for  $u$  now provided, there is now no reason to discuss  
65 obtaining the  $u$  field by finite-differencing the streamfunction. We have omitted such prose from  
66 the revised manuscript.

67

68 **4. Section 3: "The surface condition on pressure is the inhomogeneous Neumann condition**  
69 **that arises from projecting the vertical equation of motion into the vertical, and imposing**  
70 **the impermeability condition (Vreman, 2014; also see our Appendix)." The sentence can be**  
71 **maintained, but a sentence should be added that, in addition, it is important that the**  
72 **discretized Poisson equation somehow incorporates the condition that  $\delta = \text{div } \mathbf{u} = 0$  on**  
73 **the wall or in the direct vicinity of the wall. This was also stressed by Vreman (and others)**  
74 **and is briefly mentioned in the appendix. It is good to include this requirement also in the**  
75 **main text. In the method of the authors the condition  $\delta = 0$  near the wall is probably**  
76 **implicitly enforced via the alternative Poisson equation, specified in the Appendix, Eq.**  
77 **(A3b). After Eq. (A3b) the authors cite the pressure Poisson equation paradox using a**  
78 **sentence of Gresho and Sani. Please mention there that Vreman has revisited this paradox**

79 **and has shown that, at least for the standard staggered method, the discretized version of**  
80 **(A3b) (with appropriate Neumann condition) is equivalent to the discretized version of**  
81 **(A3a) supplemented with the condition that  $\text{div}(\text{Laplacian}(u))=0$  in the direct vicinity of the**  
82 **wall. Equipped with the latter the condition, the diffusion equation  $d \text{ delta}/dt = \nu * \text{ Laplacian}(\text{delta})$  leads to  $\text{delta}=0$  for all time.**

84 Yes, the divergence-free condition near the wall is enforced via the alternative Poisson  
85 equation (A3b). We have modified the sentence right after (A3b) to emphasize that this  
86 alternative Poisson equation assures that (A2) (the divergence-free condition) is satisfied.

87 Since we want section 3 to focus on the verification tests, we did not want to divert too  
88 much attention in that section to the technical details of the pressure equation, pressure boundary  
89 condition, and related topics. However, we agree that these details are certainly important and  
90 should be clearly discussed. So, as a compromise, we modified a sentence in section 3 to read:  
91 "The pressure is diagnosed from a Poisson equation (equation (3b), discussed in the  
92 Appendix),..." Then, in the Appendix we modified the sentence about (A3b) enforcing the  
93 divergence-free condition (the modification described in the paragraph above) and added two  
94 sentences to the discussion of (A3b) along the lines suggested by the referee. Then, after those  
95 two new sentences, we end the paragraph with: "We note that (A3b) is the form adopted in our  
96 numerical code."

97  
98 **5. Section 3: The numerical solutions are obtained on an un-staggered grid. Please explain**  
99 **what was done to prevent odd-even decoupling of the pressure. Was the Rhie-Chow**  
100 **interpolation method used, for example?**

101 The numerical solutions are obtained on a staggered (Arakawa C) grid so no decoupling  
102 of the pressure was occurring/noticed. We now mention "staggered (Arakawa C) grid" in the  
103 discussion of the DNS code in section 3.

104  
105 **6. Section 3: Please explain the meaning of the abbreviations HNC and INC (I guess**  
106 **homogeneous Neumann condition and inhomogeneous Neumann condition).**

107 Yes, HNC is our acronym for homogeneous Neumann condition and INC is our  
108 acronym for inhomogeneous Neumann condition. We now introduce these acronyms  
109 near the end of the second paragraph of section 3.

110 Additional modifications to the manuscript (i.e., not made in  
111 response to the reviewers' comments)

112

113 Please note that the third author would like his middle initial "A" included in his name:  
114 Jeremy A. Gibbs.

115

116 We have added a new reference: Egger (1981). The Egger study was related to ours in  
117 that it was concerned with a linear analysis of the 2D Boussinesq governing equations  
118 for thermally driven flow. Egger's analysis was largely for slope flows, though with flat  
119 terrain (our focus) considered as a special case. However, Egger outlines how to get the  
120 analytical solution but does not actually provide the final analytical solution. We  
121 mention this Egger study in the second paragraph of Section 1. We also mention it in  
122 the paragraph right after (2.8): the restriction on acceptable surface buoyancies  
123 described in that paragraph was first noted by Egger, though without details.

124

125 A correction was made to the original equations (2.39) and (2.40) [these now appear as  
126 equations (2.40) and (2.42), respectively]. The factor  $k^{1/3}$  in the denominator of the  
127 term in front of the summation in (2.39) and the factor  $k^{2/3}$  in the numerator of the  
128 term in front of the summation in (2.40) should be kept inside the summations. These  
129 factors were treated correctly in the computer code, so none of the presented results  
130 were affected.

131

132 Section 3. We now make the number of points in the  $x$  and  $z$  direction unambiguous:  
133 instead of writing the number of points in test A-1 as (513, 1025) we write, "...consisted  
134 of 513 points in the  $x$  direction and 1025 points in the  $z$  direction,..." Similarly, for test  
135 A-2, we now write, "...was generated with 2049 points in the  $x$  direction and 513 points

136 in the  $z$  direction,..."

137

138 In the Appendix we now write the time step as  $\Delta t$  instead of  $\delta t$  since the symbol  $\delta$   
139 has already been used to represent the divergence of the velocity field.

140

141 In several places in the manuscript we now use bold to indicate the vector  $\mathbf{u}$  (formerly  
142 we used  $\vec{u}$ ).

143

144 We have slightly modified the acknowledgements statement (we now thank the  
145 anonymous reviewer).

146

147        **An analytical verification test for numerically simulated convective flow**

148                                **above a thermally heterogeneous surface**

149                                by Alan Shapiro, Evgeni Fedorovich, and Jeremy A. Gibbs

150

151    **Abstract.** An analytical solution of the Boussinesq equations for the motion of a  
152    viscous stably stratified fluid driven by a surface thermal forcing with large horizontal  
153    gradients (step changes) is obtained. This analytical solution is one of the few available  
154    for wall-bounded buoyancy-driven flows. The solution can be used to verify that  
155    computer codes for Boussinesq fluid system simulations are free of errors in formulation  
156    of wall boundary conditions and to evaluate the relative performances of competing  
157    numerical algorithms. Because the solution pertains to flows driven by a surface thermal  
158    forcing, one of its main applications may be for testing the no-slip, impermeable wall  
159    boundary conditions for the pressure Poisson equation. Examples of such tests are  
160    presented.

## 161 1 Introduction

162 Thermal disturbances associated with variations in underlying surface properties can  
163 drive local circulations in the atmospheric boundary layer (Atkinson, 1981; Briggs, 1988;  
164 Hadfield et al., 1991; Segal and Arritt, 1992; Simpson, 1994; Mahrt et al., 1994; Pielke,  
165 2001; McPherson, 2007; Kang et al., 2012) and affect the development of the convective  
166 boundary layer (Patton et al., 2005; van Heerwaarden et al., 2014). Computational fluid  
167 dynamics (CFD) codes for modeling such flows commonly solve the Boussinesq  
168 equations of motion and thermal energy for a viscous/diffusive stably stratified fluid. In  
169 this paper we present an analytical solution of the Boussinesq equations for flows driven  
170 by a surface thermal forcing with large gradients (step changes) in the horizontal. The  
171 solution can be used to verify that CFD codes for Boussinesq fluid system simulations  
172 are free of errors, and to evaluate the relative performances of competing numerical  
173 algorithms. Such verification procedures are important in the development of CFD  
174 models designed for research, operational, and classroom applications.

175         We solve the linearized Navier-Stokes and thermal energy equations analytically  
176 for the case where the surface buoyancy varies laterally as a square wave (Fig. 1).  
177 Attention is restricted to the steady state. No boundary-layer approximations are made;  
178 the solution is non-hydrostatic, and both horizontal and vertical derivatives are included  
179 in the viscous stress and thermal diffusion terms. The solution is similar to that of  
180 Axelsen et al. (2010) for katabatic flow above a cold strip, but is easier to evaluate (no



181 slope present) and applies to the more general scenario where the viscosity and  
182 diffusivity coefficients can differ. The flow is also similar to a special case (no slope)  
183 considered by Egger (1981), although a final analytical solution was not provided in  
184 that study. Strictly speaking, the linearized Navier-Stokes equations apply to a class of  
185 very low Reynolds number motions known as creeping flows. Such flows appear in  
186 studies of lubrication, locomotion of microorganisms, lava flow, and flow in porous  
187 media. Of course, for the task at hand, if our linear solution is to serve as a benchmark  
188 for a nonlinear numerical model solution, it is essential that the parameter space be  
189 restricted to values for which the model's nonlinear terms are negligible.

190       Because the solution pertains to flows driven by a surface thermal forcing, one of  
191 its main applications may be as a test for surface boundary conditions in the pressure  
192 Poisson equation. In models of atmospheric boundary layer flows, the buoyancy is a  
193 major contributor to the forcing term in the Poisson equation and also appears in the  
194 associated surface boundary condition. The pressure boundary condition on a solid  
195 boundary in incompressible (Boussinesq) fluid flows is an important and complex issue  
196 that has long been fraught with technical difficulties and controversies (Strikwerda,  
197 1984; Orszag et al., 1986; Gresho and Sani, 1987; Gresho, 1990; Temam, 1991; Henshaw,  
198 1994; Petersson, 2001; Sani et al., 2006; Rempfer, 2006; Guermond et al., 2006;  
199 Nordström et al., 2007; Shirokoff and Rosales, 2011; Hosseini and Feng, 2011; Vreman,  
200 2014). Typical fractional-step solution methodologies and associated pressure (or

201 pseudo-pressure) boundary-condition implementations are often verified using various  
202 prototypic flows such as Poiseuille flows, lid-driven cavity flows, flows over cylinders or  
203 bluff bodies, viscously decaying vortices, and dam-break flows. We are unaware of  
204 verification tests in which flows were driven by a heterogeneous surface buoyancy  
205 forcing. Our solution is designed to fill this gap.

206         The analytical solution is derived in Sect. 2. In Sect. 3, this solution is compared  
207 to numerically simulated fields in a steady state. Two versions of a numerical code are  
208 run: a version in which the correct surface pressure boundary condition is applied, and a  
209 version in which the pressure condition is mis-specified. A summary follows in Sect. 4.

210

## 211 **2 Analytical solution**

212 We derive the solution for steady flow over an underlying surface along which the  
213 buoyancy varies laterally as a single harmonic function. This single-harmonic solution is  
214 then used as a building block in a Fourier representation of the square-wave solution.

215

### 216 **2.1 Governing equations**

217 Consider the flow of a viscous stably stratified fluid that fills the semi-infinite domain  
218 above a solid horizontal surface (placed at  $z = 0$ ). This surface undergoes a steady  
219 thermal forcing that varies periodically in the right-hand Cartesian  $x$  direction, but is  
220 independent of the  $y$  direction. The two-dimensional  $(x, z)$  flow is periodic in  $x$ , and

221 satisfies the linearized (assuming the disturbance is of small amplitude) governing  
 222 equations under the Boussinesq approximation,

$$223 \quad 0 = -\frac{\partial \Pi}{\partial x} + \nu \nabla^2 u, \quad (2.1)$$

$$224 \quad 0 = -\frac{\partial \Pi}{\partial z} + b + \nu \nabla^2 w, \quad (2.2)$$

$$225 \quad 0 = -N^2 w + \alpha \nabla^2 b, \quad (2.3)$$

$$226 \quad \frac{\partial u}{\partial x} + \frac{\partial w}{\partial z} = 0. \quad (2.4)$$

227 Apart from notational differences, (2.1)–(2.4) are the two-dimensional steady state  
 228 versions of (55)–(57) of Sect. II of Chandrasekhar (1961). Equations (2.1) and (2.2) are  
 229 the horizontal ( $x$ ) and vertical ( $z$ ) equations of motion, respectively, (2.3) is the thermal  
 230 energy equation (differential form of the first law of thermodynamics) expressed in  
 231 terms of the buoyancy variable (defined below), and (2.4) is the incompressibility  
 232 condition. Here  $u$  and  $w$  are the horizontal and vertical velocity components,  $\Pi \equiv$   
 233  $[p - p_e(z)]/\rho_w$  is the kinematic pressure perturbation [ $p$  is pressure,  $p_e(z)$  is pressure in a  
 234 hydrostatic environmental state in which the density profile is  $\rho_e(z)$ ,  $\rho_w$  is a constant  
 235 reference density, say,  $\rho_e(0)$ ], and  $b \equiv -g[\rho - \rho_e(z)]/\rho_w$  is the buoyancy, where  $\rho$  is the  
 236 actual density, and  $g$  is the acceleration due to gravity. The Brunt-Väisälä frequency  
 237  $N \equiv \sqrt{-(g/\rho_w)d\rho_e/dz}$  of the ambient fluid (Kundu 1990), kinematic viscosity  $\nu$ , and  
 238 thermal diffusivity  $\alpha$  are taken constant.

239 We obtain our solution using a standard vorticity/streamfunction formulation.

240 Cross-differentiating (2.1) and (2.2) yields the vorticity equation,

$$241 \quad 0 = -\frac{\partial b}{\partial x} + \nu \nabla^2 \eta, \quad (2.5)$$

242 where  $\eta \equiv \partial u / \partial z - \partial w / \partial x$  is the vorticity. Eliminating  $b$  from (2.3) and (2.5) yields

$$243 \quad \nabla^4 \eta = \frac{N^2}{\nu \alpha} \frac{\partial w}{\partial x}. \quad (2.6)$$

244 Introducing a streamfunction  $\psi$  defined through

$$245 \quad u = \partial \psi / \partial z, \quad w = -\partial \psi / \partial x, \quad (2.7)$$

246 guarantees that (2.4) is satisfied, and transforms (2.6) into a single equation for  $\psi$ ,

$$247 \quad \nabla^6 \psi + \frac{N^2}{\nu \alpha} \frac{\partial^2 \psi}{\partial x^2} = 0. \quad (2.8)$$

248 The dependent variables are assumed to vanish far above the surface ( $z \rightarrow \infty$ ). On the

249 surface we apply no-slip ( $u = 0$ ) and impermeability ( $w = 0$ ) conditions, and specify a

250 periodic (in  $x$ ) buoyancy distribution. As we will now see, restricting the dependent

251 variables to steady periodic forms that vanish as  $z \rightarrow \infty$  also restricts acceptable

252 distributions of the surface buoyancy. The restriction was first noted by Egger (1981,

253 Sect. 3c), though without details. Averaging (2.3) over one period (using  $w = -\partial \psi / \partial x$ )

254 yields  $d^2 \bar{b} / dz^2 = 0$ , which integrates to  $\bar{b} = A + Bz$  ( $\bar{b}$  is the average of  $b$ ;  $A$  and  $B$  are

255 constants). Taking  $b \rightarrow 0$  as  $z \rightarrow \infty$ , implies that  $\bar{b} \rightarrow 0$  as  $z \rightarrow \infty$ , in which case  $A =$

256  $B = 0$ , and  $\bar{b}(z) = 0$ . In particular, at the surface,  $\bar{b}(0) = 0$ . If a surface distribution

257  $b(x,0)$  violates this condition, the ground acts as a net heat source/sink. In an unsteady  
 258 model, such a source/sink would force a continually upward-developing disturbance, and  
 259 a steady state could never be attained.

260

## 261 2.2 Single-harmonic forcing

262 For a surface buoyancy of the form  $b(x,0) \propto \sin kx$ , (2.3) indicates that  $\psi$  is of the form

$$263 \quad \psi = A(z) \cos kx. \quad (2.9)$$

264 Application of (2.9) in (2.8) yields

$$265 \quad \left( \frac{d^2}{dz^2} - k^2 \right)^3 A - \frac{N^2 k^2}{\nu \alpha} A = 0, \quad (2.10)$$

266 which has solutions of the form  $A \propto e^{Mz}$  for  $M$  satisfying

$$267 \quad (M^2 - k^2)^3 = \frac{N^2 k^2}{\nu \alpha}. \quad (2.11)$$

268 Taking the one-third power of (2.11) yields a useful intermediate result:

$$269 \quad M^2 - k^2 = \frac{N^{2/3} k^{2/3}}{\nu^{1/3} \alpha^{1/3}} e^{2n\pi i/3}, \quad (2.12)$$

270 where  $n$  is an integer. Rearranging (2.12) and taking the square root yields

$$271 \quad M = \pm \sqrt{k^2 + \frac{N^{2/3} k^{2/3}}{\nu^{1/3} \alpha^{1/3}} e^{2n\pi i/3}}. \quad (2.13)$$

272 Equation (2.13) furnishes six roots, two for each of  $n = 0, 1, 2$ . To ensure that  $A(z) \rightarrow 0$

273 as  $z \rightarrow \infty$ , we reject the roots with a positive real part. With the radicand of (2.13)

274 expressed in polar form, the physically acceptable roots are

$$275 \quad M_0 = -\sqrt{k^2 + \frac{N^{2/3}k^{2/3}}{\nu^{1/3}\alpha^{1/3}}}, \quad (n = 0), \quad (2.14a)$$

$$276 \quad M_1 = -r^{1/2}e^{i\phi/2}, \quad (n = 1), \quad (2.14b)$$

$$277 \quad M_2 = -r^{1/2}e^{-i\phi/2}, \quad (n = 2), \quad (2.14c)$$

278 where the subscript on  $M$  denotes the associated value of  $n$ , and  $r$  and  $\phi$  are defined by

$$279 \quad r \equiv \sqrt{\left[ k^2 + \frac{N^{2/3}k^{2/3}}{\nu^{1/3}\alpha^{1/3}} \cos\left(\frac{2\pi}{3}\right) \right]^2 + \left[ \frac{N^{2/3}k^{2/3}}{\nu^{1/3}\alpha^{1/3}} \sin\left(\frac{2\pi}{3}\right) \right]^2}, \quad (2.15)$$

$$280 \quad \cos \phi = \frac{1}{r} \left[ k^2 + \frac{N^{2/3}k^{2/3}}{\nu^{1/3}\alpha^{1/3}} \cos\left(\frac{2\pi}{3}\right) \right], \quad \sin \phi = \frac{1}{r} \left( \frac{N^{2/3}k^{2/3}}{\nu^{1/3}\alpha^{1/3}} \right) \sin\left(\frac{2\pi}{3}\right) > 0. \quad (2.16)$$

281 While solving (2.16) for  $\phi$ , care must be taken when evaluating arcsin or arccos

282 functions that  $\phi$  appears in the correct quadrant ( $\phi$  should be in quadrant I or II so

283  $\phi/2$  should always be in quadrant I). Also note from (2.14b) and (2.14c) that  $M_2$  is the

284 complex conjugate of  $M_1$  ( $M_2 = M_1^*$ ), a fact that will often be used below.

285 With the general solution for  $\psi$  written as

$$286 \quad \psi = (B e^{M_0 z} + C e^{M_1 z} + D e^{M_2 z}) \cos kx, \quad (2.17)$$

287 where  $B$ ,  $C$ , and  $D$  are constants, the vorticity becomes,

$$288 \quad \eta = \left[ B(M_0^2 - k^2) e^{M_0 z} + C(M_1^2 - k^2) e^{M_1 z} + D(M_2^2 - k^2) e^{M_2 z} \right] \cos kx, \quad (2.18)$$

289 and the buoyancy follows from (2.3) as

290 
$$b = \frac{kN^2}{\alpha} \left( \frac{B}{M_0^2 - k^2} e^{M_0 z} + \frac{C}{M_1^2 - k^2} e^{M_1 z} + \frac{D}{M_2^2 - k^2} e^{M_2 z} \right) \sin kx + b_h, \quad (2.19)$$

291 where  $\nabla^2 b_h = 0$ . In view of (2.12), equation (2.19) becomes

292 
$$b = \frac{k^{1/3} \nu^{1/3} N^{4/3}}{\alpha^{2/3}} (B e^{M_0 z} + e^{-2\pi i/3} C e^{M_1 z} + e^{-4\pi i/3} D e^{M_2 z}) \sin kx + b_h. \quad (2.20)$$

293 Applying (2.18) and (2.20) in (2.5) yields an equation for  $\partial b_h / \partial x$ , which upon use of

294 (2.12) and  $M_2 = M_1^*$  reduces to  $\partial b_h / \partial x = 0$ . So  $b_h$  is, at most, a function of  $z$ . Since

295  $\nabla^2 b_h = 0$ ,  $b_h$  is, at most, a linear function of  $z$ , and since  $b$  should vanish as  $z \rightarrow \infty$ ,

296 that linear function must be 0. Thus,  $b_h = 0$ .

297 The pressure follows from (2.1) and (2.12) as

298 
$$\Pi = \frac{\nu^{2/3} N^{2/3}}{k^{1/3} \alpha^{1/3}} (B M_0 e^{M_0 z} + C M_1 e^{2\pi i/3} e^{M_1 z} + D M_2 e^{4\pi i/3} e^{M_2 z}) \sin kx + G(z), \quad (2.21)$$

299 where  $G(z)$  is a function of integration. Applying (2.21) in (2.2), and using (2.11) yields

300  $dG/dz = 0$ , so  $G$  is constant. For  $\Pi$  to vanish as  $z \rightarrow \infty$ , this constant must be zero.

301 The surface conditions determine  $B$ ,  $C$ , and  $D$ . The surface buoyancy is

302 
$$b(x, 0) = b_0 \sin kx, \quad (2.22)$$

303 where  $b_0$  is a constant forcing amplitude. Application of (2.20) in (2.22) yields

304 
$$B + e^{-2\pi i/3} C + e^{-4\pi i/3} D = \frac{b_0 \alpha^{2/3}}{k^{1/3} \nu^{1/3} N^{4/3}}. \quad (2.23)$$

305 In view of (2.7) and (2.17), the impermeability condition  $w(x, 0) = 0$  and no-slip

306 condition  $u(x,0) = 0$  yield

$$307 \quad B + C + D = 0, \quad (2.24)$$

$$308 \quad BM_0 + CM_1 + DM_2 = 0. \quad (2.25)$$

309 Straightforward but lengthy manipulations yield the solution of (2.23)–(2.25):

$$310 \quad B = - \left( \frac{b_0 \alpha^{2/3}}{\sqrt{3} k^{1/3} \nu^{1/3} N^{4/3}} \right) \frac{2r^{1/2} \sin(\phi/2)}{M_0 + 2r^{1/2} \cos(\pi/3 + \phi/2)}, \quad (2.26)$$

$$311 \quad C = -i \left( \frac{b_0 \alpha^{2/3}}{\sqrt{3} k^{1/3} \nu^{1/3} N^{4/3}} \right) \frac{M_2 - M_0}{M_0 + 2r^{1/2} \cos(\pi/3 + \phi/2)}, \quad (2.27)$$

$$312 \quad D = i \left( \frac{b_0 \alpha^{2/3}}{\sqrt{3} k^{1/3} \nu^{1/3} N^{4/3}} \right) \frac{M_1 - M_0}{M_0 + 2r^{1/2} \cos(\pi/3 + \phi/2)}. \quad (2.28)$$

313 Applying (2.26)–(2.28) in (2.17), (2.20), and (2.18), with (2.12) used in the latter  
 314 equation, and noting that  $B$  is real, while  $D = C^*$  (since  $M_2 = M_1^*$ ), we obtain

$$315 \quad b = \frac{2b_0}{\sqrt{3}} \frac{e^{-Z_c} [\mu \cos(Z_s + \pi/6) + \cos(Z_s + \pi/6 + \phi/2)] - e^{M_0 z} \sin(\phi/2)}{\mu + 2 \cos(\pi/3 + \phi/2)} \sin kx, \quad (2.29)$$

$$316 \quad \psi = \frac{2b_0 \alpha^{2/3}}{\sqrt{3} k^{1/3} \nu^{1/3} N^{4/3}} \frac{e^{-Z_c} [\mu \sin Z_s + \sin(Z_s + \phi/2)] - e^{M_0 z} \sin(\phi/2)}{\mu + 2 \cos(\pi/3 + \phi/2)} \cos kx, \quad (2.30)$$

317 where

$$318 \quad Z_s \equiv z r^{1/2} \sin(\phi/2), \quad Z_c \equiv z r^{1/2} \cos(\phi/2), \quad \mu \equiv M_0 / r^{1/2}. \quad (2.31)$$

319 Application of (2.30) in (2.7) yields the velocity components as



320 
$$u = \frac{2b_0 \alpha^{2/3} r^{1/2}}{\sqrt{3} k^{1/3} \nu^{1/3} N^{4/3}} \frac{e^{-Z_c} [\mu \sin(\phi/2 - Z_s) - \sin Z_s] - \mu e^{M_0 z} \sin(\phi/2)}{\mu + 2 \cos(\pi/3 + \phi/2)} \cos kx \quad (2.32)$$

321 
$$w = \frac{2b_0 \alpha^{2/3} k^{2/3}}{\sqrt{3} \nu^{1/3} N^{4/3}} \frac{e^{-Z_c} [\mu \sin Z_s + \sin(Z_s + \phi/2)] - e^{M_0 z} \sin(\phi/2)}{\mu + 2 \cos(\pi/3 + \phi/2)} \sin kx. \quad (2.33)$$

322

### 323 2.3 Piecewise constant (square wave) forcing

324 Next, consider the case where the surface buoyancy varies horizontally as a square

325 wave, with a distribution over one period  $L$  given by

326 
$$b(x, 0) = \begin{cases} b_{\max}, & 0 < x < L/2, \\ -b_{\max}, & L/2 < x < L. \end{cases} \quad (2.34)$$

327 Such a distribution can be expressed as the Fourier series:

328 
$$b(x, 0) = \sum_{n=1}^{\infty} b_n \sin\left(\frac{n\pi x}{L}\right), \quad (2.35)$$

329 
$$b_n = \frac{2}{L} \int_0^L b(x, 0) \sin\left(\frac{n\pi x}{L}\right) dx. \quad (2.36)$$

330 Application of (2.34) in (2.36) yields

331 
$$b_n = \frac{2b_{\max}}{n\pi} [1 - 2 \cos(n\pi/2) + \cos(n\pi)]. \quad (2.37)$$

332 The solutions for  $b$ ,  $\psi$ ,  $u$ , and  $w$  can then be written as summations over the single-

333 harmonic solutions (2.29), (2.30), (2.32), and (2.33), with  $k$  related to  $n$  by

334 
$$k = \frac{n\pi}{L}, \quad (2.38)$$

335 and with  $b_0$  replaced by  $b_n$  :

$$336 \quad b = \frac{2}{\sqrt{3}} \sum_{n=1}^{\infty} b_n \frac{e^{-Z_c} [\mu \cos(Z_s + \pi/6) + \cos(Z_s + \pi/6 + \phi/2)] - e^{M_0 z} \sin(\phi/2)}{\mu + 2 \cos(\pi/3 + \phi/2)} \sin\left(\frac{n\pi x}{L}\right), \quad (2.39)$$

$$337 \quad \psi = \frac{2\alpha^{2/3}}{\sqrt{3} \nu^{1/3} N^{4/3}} \sum_{n=1}^{\infty} \frac{b_n}{k^{1/3}} \frac{e^{-Z_c} [\mu \sin Z_s + \sin(Z_s + \phi/2)] - e^{M_0 z} \sin(\phi/2)}{\mu + 2 \cos(\pi/3 + \phi/2)} \cos\left(\frac{n\pi x}{L}\right), \quad (2.40)$$

$$338 \quad u = \frac{2\alpha^{2/3}}{\sqrt{3} \nu^{1/3} N^{4/3}} \sum_{n=1}^{\infty} b_n \frac{r^{1/2}}{k^{1/3}} \frac{e^{-Z_c} [\mu \sin(\phi/2 - Z_s) - \sin Z_s] - \mu e^{M_0 z} \sin(\phi/2)}{\mu + 2 \cos(\pi/3 + \phi/2)} \cos\left(\frac{n\pi x}{L}\right), \quad (2.41)$$

$$339 \quad w = \frac{2\alpha^{2/3}}{\sqrt{3} \nu^{1/3} N^{4/3}} \sum_{n=1}^{\infty} b_n k^{2/3} \frac{e^{-Z_c} [\mu \sin Z_s + \sin(Z_s + \phi/2)] - e^{M_0 z} \sin(\phi/2)}{\mu + 2 \cos(\pi/3 + \phi/2)} \sin\left(\frac{n\pi x}{L}\right). \quad (2.42)$$

340

### 341 **3 Verification tests**

342 A solution of the linearized equations may be used to verify a nonlinear code if the  
 343 nonlinear terms are sufficiently small. Unfortunately, *a priori* estimates of such terms  
 344 expressed, for example, through a Reynolds number, are not straightforward since the  
 345 relevant velocity and length scales in our problem are only evident after a solution has  
 346 been obtained. We thus seek an appropriate set of test parameters through trial and  
 347 error, guided by *a posteriori* linear solution estimates of the terms  $\mathbf{u} \cdot \nabla b$  and  $\mathbf{u} \cdot \nabla \eta$   
 348 [ $\mathbf{u} = (u, w)$ ] present in nonlinear versions of (2.3) and (2.5), respectively. Specifically, for  
 349 any computed candidate solution, we formed the ratios of the largest values of those  
 350 nonlinear terms to the largest values of the corresponding linear terms, that is, the

351 terms actually present in (2.3) and (2.5). We need only consider one such linear term  
 352 per ratio since (2.3) and (2.5) are comprised of two terms of equal magnitude. A  
 353 solution was deemed to be sufficiently linear if

$$354 \quad R_\eta \equiv \frac{\max|\mathbf{u} \cdot \nabla \eta|}{\max|\partial b / \partial x|} < \varepsilon, \quad \text{and} \quad R_b \equiv \frac{\max|\mathbf{u} \cdot \nabla b|}{\max|\alpha \nabla^2 b|} < \varepsilon, \quad (3.1)$$

355 where  $\varepsilon$  ( $\ll 1$ ) is a prescribed threshold. The suitability of this approach was  
 356 confirmed by the very close agreement between the analytical solutions and the  
 357 numerical solutions obtained with the correct surface pressure condition.

358         The numerical model employed in our tests is a variant of a direct numerical  
 359 simulation (DNS) code used in the boundary-layer and slope-flow studies of Fedorovich  
 360 et al. (2001), Fedorovich and Shapiro (2009a,b), and Shapiro and Fedorovich (2013,  
 361 2014). The model solves the Boussinesq governing equations on a staggered (Arakawa  
 362 C) grid. Although designed for three-dimensional simulations, the model was run in a  
 363 two-dimensional ( $x, z$ ) mode. The overall solution procedure is patterned on a fractional  
 364 step method proposed by Chorin (1968). In our version, the prognostic equations are  
 365 integrated using a filtered leapfrog scheme with explicit treatment of the viscous term.  
 366 The pressure is diagnosed from a Poisson equation (equation (A3b), discussed in the  
 367 Appendix), which is solved using a fast Fourier transform technique in horizontal  
 368 planes, and a tridiagonal matrix inversion in the vertical. The surface condition on  
 369 pressure is the inhomogeneous Neumann condition (INC) that arises from projecting the

370 vertical equation of motion into the vertical, and imposing the impermeability condition  
371 (Vreman, 2014; also see the Appendix). We also run a version of the code in which the  
372 surface pressure condition is mis-specified as a homogeneous Neumann condition (HNC).  
373 We hasten to add, however, that our implementation of the HNC may be quite different  
374 from implementations described in the literature. We elaborate on these technical  
375 differences and review general aspects of the problem of surface pressure specification in  
376 the Appendix.

377 The analytical solution was evaluated on an un-staggered  $(x, z)$  grid extending  
378 over one period of the square wave ( $x = 0$  to  $x = L$ ). The series were truncated at  
379 50000 terms. The governing parameters were adjusted so that the linearity criteria  
380 were satisfied in comparisons with  $\varepsilon = 5 \times 10^{-3}$ .

381 In the first test, we set  $\nu = \alpha = 0.001 \text{ m}^2 \text{ s}^{-1}$ ,  $N = 0.02 \text{ s}^{-1}$ ,  $L = 5.12 \text{ m}$ , and  $b_{\max}$   
382  $= 1 \times 10^{-5} \text{ m s}^{-2}$ . For the analytical solution A-1, the  $(x, z)$  grid consisted of 513 points  
383 in the  $x$  direction and 1025 points in the  $z$  direction, with grid spacings  
384  $\Delta x = \Delta z = 0.01 \text{ m}$ . The linearity criteria (3.1) were satisfied with  $R_\eta \cong 8.2 \times 10^{-5}$  and  
385  $R_b \cong 2.8 \times 10^{-3}$ . The analytical  $b$  and  $w$  fields shown in Fig. 2 depict a broad zone of  
386 ascent above the warm surface and a compensating zone of descent over the cold  
387 surface, roughly for  $z < 1.8 \text{ m}$ . In the upper part of these zones (at roughly  
388  $0.9 \text{ m} < z < 1.8 \text{ m}$ ), adiabatic expansion/compression has reversed the senses of the

389 buoyancy fields. Surprisingly, the numerical fields in the inhomogeneous INC-1 and  
 390 homogeneous HNC-1 cases are very similar to each other and to the A-1 fields. The  $u$   
 391 fields from A-1, INC-1, and HNC-1 shown in Fig. 3 are visually indistinguishable from  
 392 one another.

393 To understand why the INC-1 and HNC-1 simulations are so similar, and to  
 394 identify simulation parameters that might evince more substantial differences, we  
 395 consider the idealized problem in which a specified buoyancy  $b = b_0 e^{-\gamma z} \sin kx$  ( $\gamma = h^{-1}$ ,  
 396 where  $h$  is the e-folding depth scale) is the only forcing term in the Poisson equation  
 397  $\nabla^2 \Pi = \partial b / \partial z$ , with Neumann surface condition  $\partial \Pi / \partial z|_0 = b(x, 0)$ . This idealized  
 398 problem is solved as

$$399 \quad \Pi_{\text{INC}}^* = \frac{b_0}{\gamma^2 - k^2} \left( k e^{-kz} - \gamma e^{-\gamma z} \right) \sin kx. \quad (3.2)$$

400 The corresponding solution obtained with the homogeneous Neumann condition,  
 401  $\partial \Pi / \partial z|_0 = 0$ , is

$$402 \quad \Pi_{\text{HNC}}^* = \frac{b_0}{\gamma^2 - k^2} \left( \frac{\gamma^2}{k} e^{-kz} - \gamma e^{-\gamma z} \right) \sin kx. \quad (3.3)$$

403 The relative error ( $RE$ ) in the vertical pressure gradient force associated with (3.2) and  
 404 (3.3), defined as the local absolute error in that force divided by the local buoyancy, is  
 405 calculated as

406 
$$RE \equiv \left| \frac{\partial \Pi_{\text{INC}}^* / \partial z - \partial \Pi_{\text{HNC}}^* / \partial z}{b} \right| = e^{(a-1)kz}, \quad (3.4)$$

407 where  $a \equiv \gamma/k$ . Written in terms of the depth scale  $h$  and wavelength  $\lambda = 2\pi/k$ ,  $a$  can  
 408 be interpreted as an aspect ratio characterizing the width to depth scales of the  
 409 disturbance,  $a = \lambda/(2\pi h) \propto \lambda\gamma$ . From (3.4) we see that  $RE$  decreases exponentially with  
 410  $z$  for disturbances characterized by small aspect ratios,  $a < 1$  (which we refer to as deep  
 411 disturbances) and increases exponentially with  $z$  for disturbances characterized by large  
 412 aspect ratios,  $a > 1$  (which we refer to as shallow disturbances). The buoyancy in Fig. 2  
 413 is suggestive of  $a < 1$ , which indicates that the first test could be classified as a deep  
 414 (error-forgiving) simulation.

415 The preceding analysis suggests that simulations with shallow thermal  
 416 disturbances ( $a > 1$ ) might yield large differences between cases with inhomogeneous  
 417 and homogeneous Neumann conditions. There did not appear to be a straightforward  
 418 way to increase the effective  $a$  by systematically varying the parameters (e.g., increasing  
 419  $L$  tended to increase the effective  $h$ ), but a set of suitable parameters were identified  
 420 through trial and error and were used as the basis for the second test case.

421 In the second test, we set  $\nu = \alpha = 0.0001 \text{ m}^2 \text{ s}^{-1}$ ,  $N = 0.2 \text{ s}^{-1}$ ,  $L = 10.24 \text{ m}$ , and  
 422  $b_{\text{max}} = 5 \times 10^{-6} \text{ ms}^{-2}$ . The analytical solution A-2 was generated with 2049 points in the  
 423  $x$  direction and 513 points in the  $z$  direction, with grid spacings of  $\Delta x = \Delta z = 0.005 \text{ m}$ .  
 424 The linearity criteria were satisfied with  $R_\eta \cong 4.8 \times 10^{-5}$  and  $R_b \cong 3.8 \times 10^{-3}$ . In

425 contrast to the counter-rotating convection rolls seen in the first test, the analytical  $b$   
426 and  $w$  fields shown in Fig. 4 depict narrow updraft/downdraft pairs straddling the  
427 buoyancy discontinuities. Between the narrow updrafts is a broad region of relatively  
428 weak ascent. The  $w$  and  $b$  fields above the cold surface are mirror images of the fields  
429 above the warm surface. Note the change in the scales of the  $x$  and (especially) the  $z$   
430 axes between Figs. 4 and 2: the low-level thermal disturbance in the second test is much  
431 shallower than the disturbance in the first test (and is suggestive of  $a > 1$ ). In this  
432 second test case we find dramatic differences between the inhomogeneous INC-2 and  
433 homogeneous HNC-2 cases. Specifically, while the INC-2 and A-2 fields are in excellent  
434 agreement, the HNC-2 fields showed no signs of even approaching a steady state. Long  
435 after the INC-2 simulation had reached a steady state, the HNC-2 fields continued to  
436 amplify and develop asymmetric structures associated with flow nonlinearities. The very  
437 close agreement between the A-2 solution and the steady state in the INC-2 simulation  
438 is shown for the  $u$  field in Fig. 5. The  $u$  field in the disastrous HNC-2 simulation, at a  
439 time when a steady state had already been attained in the INC-2 simulation, is shown  
440 in Fig. 6.

441

#### 442 **4 Summary**

443 The linearized Boussinesq equations for the motion of a viscous stably stratified fluid  
444 are solved analytically for a surface buoyancy that varies laterally as a square wave.

445 The solution describes two-dimensional laminar convective structures such as thermal  
446 convective rolls and updraft/downdraft pairs. The main applications of the solution may  
447 be in code verification and the evaluation of different implementations of the surface  
448 pressure condition for the pressure Poisson equation. Tests have been conducted for  
449 cases where the aspect ratios of the thermal disturbance have been large and small.  
450 With attention restricted to disturbances of sufficiently small amplitude, the linear  
451 solution and numerically simulated fields with the inhomogeneous Neumann condition  
452 for pressure (which is appropriate in the context of the particular fractional step  
453 procedure adopted in our DNS code) have been found to be in excellent agreement for  
454 both tests. However, in tests with a mis-specified Neumann condition, an excellent  
455 agreement with the analytical solution has been found only for the deep (small aspect  
456 ratio) disturbance case; errors in the shallow (large aspect ratio) disturbance case have  
457 been catastrophic.



458 **Appendix A: Comment on the pressure condition at a lower solid surface**

459 Consider a three-dimensional Boussinesq system with equation of motion,

$$460 \quad \frac{\partial \mathbf{u}}{\partial t} = -\nabla \Pi + \nu \nabla^2 \mathbf{u} + \mathbf{F}. \quad (\text{A1})$$

461 Here  $\mathbf{u} = (u, v, w)$  is the three-dimensional velocity vector,  $\Pi$  is a kinematic pressure  
 462 perturbation,  $\nu$  is the kinematic viscosity coefficient, and  $\mathbf{F}$  is the sum of nonlinear  
 463 acceleration and buoyancy terms. Applying the incompressibility condition,

$$464 \quad \nabla \cdot \mathbf{u} = 0, \quad (\text{A2})$$

465 in the equation that results from taking the divergence of (A1) (e.g., Orszag et al., 1986)  
 466 yields the Poisson equation,

$$467 \quad \nabla^2 \Pi = \nabla \cdot \mathbf{F}. \quad (\text{A3a})$$

468 Although (A1) and (A2) imply (A3a), the reverse statement is not generally true.  
 469 Indeed, eliminating  $\Pi$  from between (A3a) and the equation arising from taking the  
 470 divergence of (A1) yields the diffusion equation  $\partial \delta / \partial t = \nu \nabla^2 \delta$  for the velocity  
 471 divergence  $\delta \equiv \nabla \cdot \mathbf{u}$ , whose solution is (A2) only if  $\delta$  is zero initially and on all  
 472 boundaries (Orszag et al., 1986; Gresho and Sani, 1987, Vreman 2014).

473 The same steps leading to (A3a) also lead to an alternative Poisson equation,

$$474 \quad \nabla^2 \Pi = \nabla \cdot (\nu \nabla^2 \mathbf{u} + \mathbf{F}). \quad (\text{A3b})$$

475 Although  $\nabla \cdot \nu \nabla^2 \mathbf{u}$  was omitted in (A3a) [this term is zero if (A2) is satisfied], without  
 476 further constraints on  $\delta$  (described above), (A2) may not be satisfied. Gresho and Sani

477 (1987) showed that the retention of  $\nabla \cdot \nu \nabla^2 \mathbf{u}$  in (A3b) assures that (A2) is satisfied,  
478 and thus leads to the paradox: "If you include it, you don't need it; if you don't include  
479 it, you need it." Vreman (2014) revisited this paradox, and showed that for a standard  
480 staggered method, the discretized form of (A3b) is equivalent to that of (A3a)  
481 supplemented with the constraint that  $\nabla \cdot \nabla^2 \mathbf{u} = 0$  ( $\nabla^2 \delta = 0$ ) on points adjacent to the  
482 solid boundary [with the same inhomogeneous Neumann boundary condition for  $\Pi$   
483 implied for (A3a) and (A3b)]. When supplemented with this  $\nabla^2 \delta = 0$  near-wall  
484 condition, the diffusion equation for  $\delta$  led to  $\delta = 0$  for all time. We note that (A3b) is  
485 the form adopted in our numerical code.

486 Evaluating the vertical component of (A1) on the surface, where the  
487 impermeability condition applies, yields the inhomogeneous Neumann condition,

$$488 \quad \left. \frac{\partial \Pi}{\partial z} \right|_0 = \nu \left. \frac{\partial^2 w}{\partial z^2} \right|_0 + F_z \Big|_0, \quad (\text{A4})$$

489 where  $w \equiv \mathbf{k} \cdot \mathbf{u}$ ,  $F_z \equiv \mathbf{k} \cdot \mathbf{F}$ ,  $\mathbf{k}$  is the upward unit vector, and  $(\ ) \Big|_0$  is a surface value. It  
490 has been argued that (A4), by itself, is not a proper boundary condition because it does  
491 not provide new information (it is not independent of the governing equations) and does  
492 not enforce the incompressibility condition (A2) at the boundary (Strikwerda, 1984;  
493 Henshaw, 1994; Sani et al., 2006). However, as pointed out by Henshaw (1994), many  
494 studies that impose (A4) (or a variant of it) also apply (A2) on the boundary.

495 In our numerical model, (A1) is integrated using a fractional step procedure with

496 explicit treatment of the viscous term. First, a provisional velocity field  $\tilde{\mathbf{u}}$  that does not  
 497 satisfy (A2) is obtained by integrating a discretized form of (A1) in which the pressure  
 498 gradient is omitted. The provisional velocity is equal to the velocity at the end of the  
 499 previous time step plus the sum of the forcing terms (nonlinear acceleration, buoyancy,  
 500 and viscous stress) multiplied by the time step  $\Delta t$ . With the forcing terms explicitly  
 501 evaluated,  $\tilde{\mathbf{u}}$  is readily computed throughout the flow domain, including on the surface,  
 502 where, in surface-forced flows, the buoyancy will make a substantial contribution. In  
 503 terms of  $\tilde{\mathbf{u}}$  and its vertical component  $\tilde{w}$ , (A3b) and (A4) become,

$$504 \quad \nabla^2 \Pi = \frac{\nabla \cdot \tilde{\mathbf{u}}}{\Delta t}, \quad (\text{A5})$$

$$505 \quad \left. \frac{\partial \Pi}{\partial z} \right|_0 - \frac{1}{\Delta t} \tilde{w} \Big|_0 = 0. \quad (\text{A6})$$

506 In the second step, a velocity field that does satisfy (A2) is obtained by solving (A5) for  
 507  $\Pi$  and then adding the pressure gradient force associated with  $\Pi$  (multiplied by  $\Delta t$ ) to  
 508  $\tilde{\mathbf{u}}$ .

509 In some explicit fractional step procedures (including the DNS code used in our  
 510 study), the problem of solving (A5) subject to (A6) with  $\tilde{\mathbf{u}}|_0$  evaluated from model data  
 511 is replaced by what appears to be an entirely different (but is actually equivalent)  
 512 problem: solving (A5) subject to the homogeneous Neumann condition,

$$513 \quad \left. \frac{\partial \Pi}{\partial z} \right|_0 = 0, \quad (\text{A7})$$

514 in concert with  $\tilde{\mathbf{u}}|_0$  being set to 0, obviating the need to calculate  $\tilde{\mathbf{u}}|_0$  from model data.  
 515 It can be shown that  $\tilde{w}|_0$  and the discretized form of  $\partial\Pi/\partial z|_0$  appear in the discretized  
 516 form of (A5) valid half a grid point above the physical surface as  $\partial\Pi/\partial z|_0 - \tilde{w}|_0/\Delta t$ , that  
 517 is, in the same combination as they appear in (A6). Thus, setting  $\tilde{w}|_0$  and  $\partial\Pi/\partial z|_0$  to 0,  
 518 is equivalent to implementing (A6) with the model-computed values of  $\tilde{w}|_0$ : the  
 519 discretized form of (A5) near the surface is the same in either case. Moreover, on the C  
 520 grid, setting the tangential components  $\tilde{u}|_0$  and  $\tilde{v}|_0$  to 0 only affects the values of  $\tilde{u}$  and  
 521  $\tilde{v}$  half a grid point beneath the physical boundary. These values do not appear in the  
 522 discretized form of (A5) at any  $z$ -level, and thus have no bearing on the solution. In  
 523 essence, the errors associated with the conflation of the two physically unjustifiable  
 524 specifications (homogeneous Neumann condition for pressure, and  $\tilde{\mathbf{u}}|_0 = 0$ ) cancel out.

525         The homogeneous Neumann condition for pressure can be the source of confusion  
 526 if the context in which the condition is applied is not made clear: it would be a correct  
 527 condition if  $\tilde{\mathbf{u}}|_0$  is set to zero (per the equivalence described above), but it would be an  
 528 incorrect condition if the explicit model-computed values of  $\tilde{\mathbf{u}}|_0$  are used. In the  
 529 experiments with the mis-specified condition described in Sect. 3, the homogeneous  
 530 condition is imposed in the latter context. Unfortunately, in many numerical model  
 531 descriptions, the nature of the surface pressure condition is left vague, for example, by

532 not indicating whether a Neumann condition is homogeneous or inhomogeneous, or, if a  
533 homogeneous Neumann condition is indicated, not mentioning how  $\tilde{\mathbf{u}}|_0$  is treated.

534 Finally, we note that in fractional step procedures that treat the viscous term  
535 implicitly (e.g., Kim and Moin, 1985; Gresho, 1990; Armfield and Street, 2002;  
536 Guermond et al., 2006, and many others), the homogeneous Neumann condition is often  
537 applied as a surface condition for a Poisson equation, but it is again different from our  
538 implementation described in Sect. 3. In the implicit treatments, the provisional velocity  
539 is obtained as the solution of a boundary value problem ( $\tilde{\mathbf{u}}|_0$  should be specified; often  
540 it is set to 0) in which the relevant Poisson equation resembles (A5) but applies to a  
541 scalar function (sometimes called a pseudo-pressure) that is not the real pressure.  
542 Temam (1991) refers to this scalar as, "... a technical quantity, a mathematical  
543 auxiliary..." and advocates that it should not even be considered as an approximation of  
544 the pressure. Interestingly, in the context of implicit treatments, the homogeneous  
545 Neumann condition on the pseudo-pressure has sometimes been implicated as corrupting  
546 solution accuracy through the development of spurious numerical boundary layers  
547 adjacent to solid boundaries (Gresho, 1990; Guermond et al., 2006; Hosseini and Feng,  
548 2011).

549

## 550 **Code availability**

551 The Fortran program used to generate output data files from the analytical solution is

552 available as a supplement to this article. That program (square.f) is configured for test  
553 A-1, but can be easily adjusted to run test A-2 or other tests. Running square.f  
554 automatically generates an output file for each dependent variable (e.g., u.dat) as well  
555 as an output file (square.out) that summarizes the test parameters and gives the  
556 computed values of the linearity ratios  $R_\eta$  and  $R_b$  defined in (3.1).

557

558 *Acknowledgements.* This research was supported by the National Science Foundation  
559 under Grant AGS-1359698. Comments by Chiel van Heerwaarden, Juan Pedro Mellado,  
560 Inanc Senocak, and an anonymous reviewer are gratefully acknowledged.

561 **References**

- 562 Armfield, S. and Street, R.: An analysis and comparison of the time accuracy of  
563 fractional-step methods for the Navier-Stokes equations on staggered grids. *Int.*  
564 *J. Numer. Methods Fluids*, 38, 255–282, 2002.
- 565 Atkinson, B.: *Meso-scale Atmospheric Circulations*. Academic Press. 495 pp., 1981.
- 566 Axelsen, S. L., Shapiro, A., and Fedorovich, E.: Analytical solution for katabatic flow  
567 induced by an isolated cold strip. *Environ. Fluid Mech.*, 10, 387–414, 2010.
- 568 Briggs, G. A.: Surface inhomogeneity effects on convective diffusion. *Boundary-Layer*  
569 *Meteorol.*, 45, 117–135, 1988.
- 570 Chandrasekhar, S.: *Hydrodynamic and Hydromagnetic Stability*. Oxford University  
571 Press. 652 pp., 1961.
- 572 Chorin, A. J.: Numerical solution of the Navier-Stokes equations. *Math. Comput.*, 22,  
573 745–762, 1968.
- 574 Egger, J.: On the linear two-dimensional theory of thermally induced slope winds. *Beitr.*  
575 *Phys. Atmosph.*, 54, 465–481, 1981.
- 576 Fedorovich, E., Nieuwstadt, F. T. M., and Kaiser, R.: Numerical and laboratory study  
577 of a horizontally evolving convective boundary layer. Part I: Transition  
578 regimes and development of the mixed layer. *J. Atmos. Sci.*, 58, 70–86, 2001.
- 579 Fedorovich, E. and Shapiro, A.: Structure of numerically simulated katabatic and  
580 anabatic flows along steep slopes. *Acta Geophys.*, 57, 981–1010, 2009a.

581 Fedorovich, E. and Shapiro, A.: Turbulent natural convection along a vertical plate  
582 immersed in a stably stratified fluid. *J. Fluid Mech.*, 636, 41–57, 2009b.

583 Gresho, P. M. and Sani, R. L.: On pressure boundary conditions for the incompressible  
584 Navier-Stokes equations. *Int. J. Numer. Methods Fluids*, 7, 1111–1145, 1987.

585 Gresho, P. M.: On the theory of semi-implicit projection methods for viscous  
586 incompressible flow and its implementation via a finite element method that also  
587 introduces a nearly consistent mass matrix. Part 1: Theory. *Int. J. Numer.*  
588 *Methods Fluids*, 11, 587–620, 1990.

589 Guermond, J. L., Mineev, P., and Shen, J.: An overview of projection methods for  
590 incompressible flows. *Comput. Methods Appl. Mech. Engrg.* 195, 6011–6045,  
591 2006.

592 Hadfield, M. G., Cotton, W. R., and Pielke, R. A.: Large-eddy simulations of thermally  
593 forced circulations in the convective boundary layer. Part I: A small-scale  
594 circulation with zero wind. *Boundary-Layer Meteorol.*, 57, 79–114, 1991.

595 Henshaw, W. D: A fourth-order accurate method for the incompressible Navier-Stokes  
596 equations on overlapping grids. *J. Comput. Phys.*, 113, 13–25, 1994.

597 Hosseini, S. M. and Feng, J. J.: Pressure boundary conditions for computing  
598 incompressible flows with SPH. *J. Comput. Phys.*, 230, 7473–7487, 2011.

599 Kang, S.-L., Lenschow, D., and Sullivan, P.: Effects of mesoscale surface thermal  
600 heterogeneity on low-level horizontal wind speeds. *Boundary-Layer Meteorol.*,



601           143, 409–432, 2012.

602 Kim, J. and Moin, P.: Application of a fractional-step method to incompressible  
603           Navier-Stokes equations. *J. Comput. Phys.*, 59, 308–323, 1985.

604 Kundu, P. K.: *Fluid Mechanics*. Academic Press. 638 pp., 1990.

605 Mahrt, L., Sun, J., Vickers, D., MacPherson, J. I., Pederson, J. R., and Desjardins, R.  
606           L.: Observations of fluxes and inland breezes over a heterogeneous surface. *J.*  
607           *Atmos. Sci.*, 51, 2484–2499, 1994.

608 McPherson, R. A.: A review of vegetation-atmosphere interactions and their influences  
609           on mesoscale phenomena. *Prog. Phys. Geog.*, 31, 261–285, 2007.

610 Nordström, J., Mattsson, K., and Swanson, C.: Boundary conditions for a divergence  
611           free velocity-pressure formulation of the Navier-Stokes equations. *J.*  
612           *Comput. Phys.*, 225, 874–890, 2007.

613 Orszag, S. A., Israeli, M., and Deville, M. O.: Boundary conditions for incompressible  
614           flows. *J. Sci. Comput.*, 1, 75–111, 1986.

615 Patton, E. G., Sullivan, P. P., and Moeng, C.-H.: The influence of idealized  
616           heterogeneity on wet and dry planetary boundary layers coupled to the land  
617           surface. *J. Atmos. Sci.*, 62, 2078–2097, 2005.

618 Petersson, N. A.: Stability of pressure boundary conditions for Stokes and Navier-  
619           Stokes equations. *J. Comput. Phys.*, 172, 40–70, 2001.

620 Pielke, R. A.: Influence of the spatial distribution of vegetation and soils on the

621 prediction of cumulus convective rainfall. *Rev. Geophys.*, 39, 151–177, 2001.

622 Rempfer, D.: On boundary conditions for incompressible Navier-Stokes problems. *Appl.*  
623 *Mech. Rev.*, 59, 107–125, 2006.

624 Segal, M. and Arritt, R. W.: Non-classical mesoscale circulations caused by surface  
625 sensible heat-flux gradients. *Bull. Amer. Meteorol. Soc.*, 73, 1593–1604, 1992.

626 Shirokoff, D. and Rosales, R. R.: An efficient method for the incompressible Navier-  
627 Stokes equations on irregular domains with no-slip boundary conditions, high  
628 order up to the boundary. *J. Comput. Phys.*, 230, 8619–8646, 2011.

629 Shapiro, A. and Fedorovich, E.: Similarity models for unsteady free convection flows  
630 along a differentially cooled horizontal surface. *J. Fluid Mech.*, 736, 444–463,  
631 2013.

632 Shapiro, A. and Fedorovich, E.: A boundary-layer scaling for turbulent katabatic flow.  
633 *Boundary-Layer Meteorol.*, 153, 1–17, 2014.

634 Simpson, J. E.: *Sea Breeze and Local Winds*. Cambridge University Press. 234 pp.,  
635 1994.

636 Temam, R.: Remark on the pressure boundary condition for the projection method.  
637 *Theoret. Comput. Fluid Dynamics*, 3, 181–184, 1991.

638 Strikwerda, J. C.: Finite difference methods for the Stokes and Navier-Stokes equations.  
639 *SIAM J. Sci. Stat. Comput.*, 5, 56–68, 1984.

640 van Heerwaarden, C. C., Mellado, J. P., and de Lozar, A.: Scaling laws for the

641 heterogeneously heated free convective boundary layer. *J. Atmos. Sci.*, 71, 3975–  
642 4000, 2014.

643 Vreman, A. W.: The projection method for the incompressible Navier-Stokes equations:  
644 The pressure near a no-slip wall. *J. Comput. Phys.*, 263, 353–374, 2014.

645

646

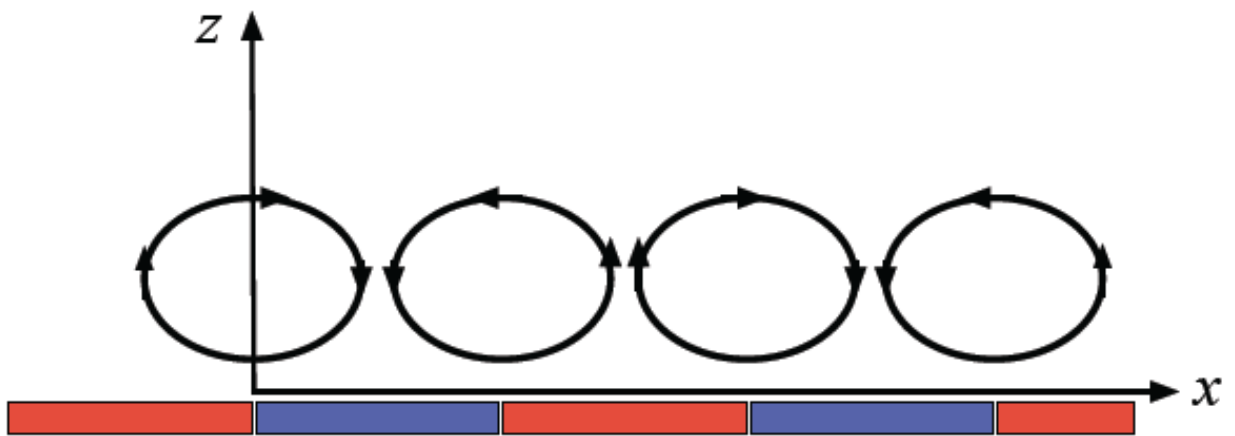
647

648

649

650

651



652

653

654 **Figure 1.** Schematic of two-dimensional  $(x, z)$  thermal convection induced by a surface

655 buoyancy that varies horizontally  $(x)$  as a square wave. Red denotes positive surface

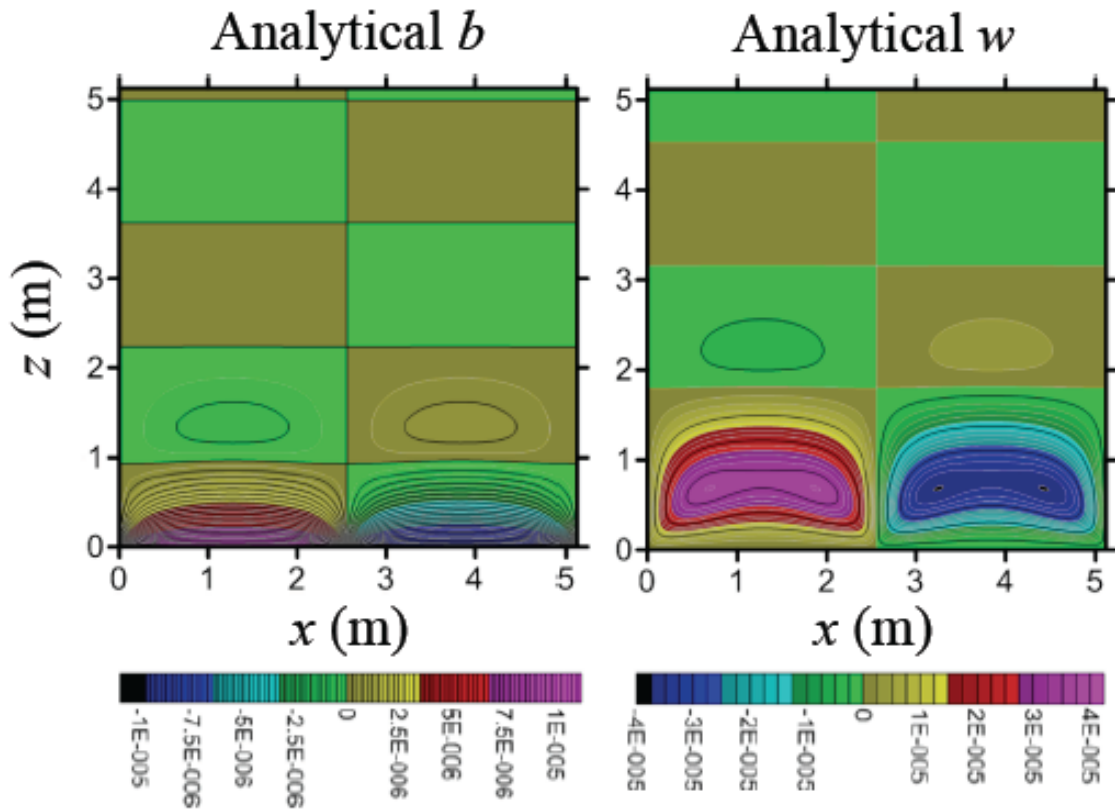
656 buoyancy, blue denotes negative surface buoyancy.

657

658

659

660



661

662

663

664 **Figure 2.** Vertical cross section of the analytical (A-1) buoyancy  $b$  and vertical velocity

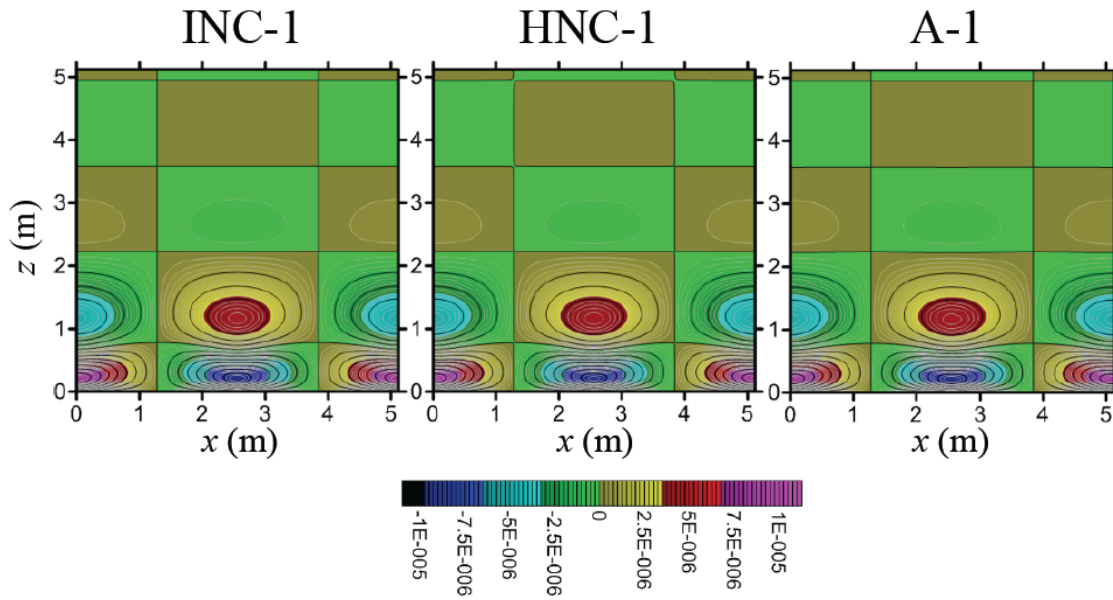
665  $w$  fields from the first test case. Color bar units are  $\text{m s}^{-2}$  for  $b$ , and  $\text{m s}^{-1}$  for  $w$ .

666

667

668

669



670

671

672

673 **Figure 3.** Vertical cross section of  $u$  from the first test case. A-1 is the analytical

674 solution. INC-1 is the numerical simulation with inhomogeneous Neumann condition for

675 pressure. HNC-1 is the numerical simulation with the homogeneous Neumann condition

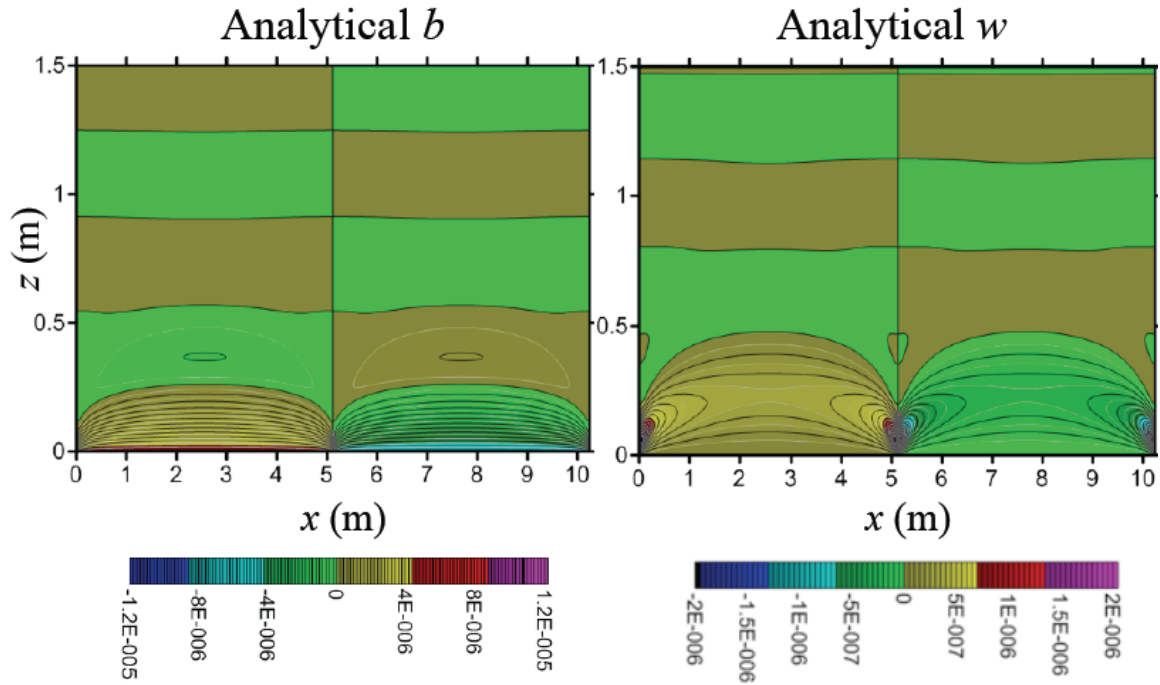
676 for pressure. Color bar units are  $\text{m s}^{-1}$ .

677

678

679

680



681

682

683

684 **Figure 4.** Vertical cross section of the analytical (A-2) buoyancy  $b$  and vertical velocity

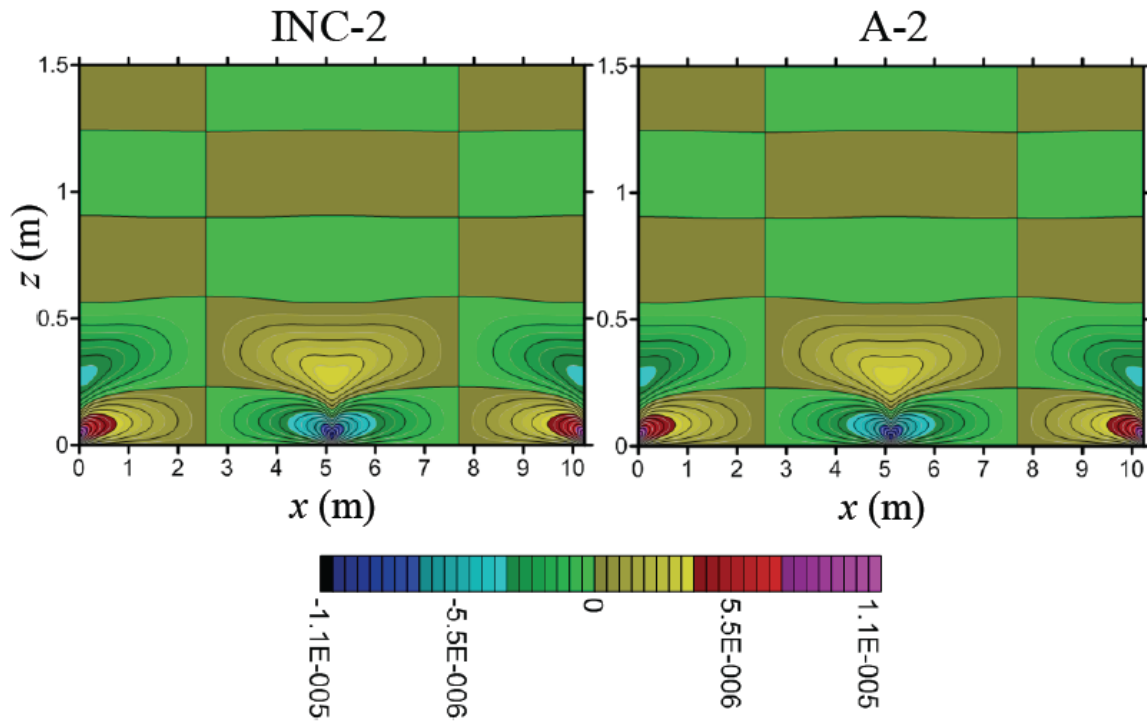
685  $w$  fields from the second test case. Color bar units are  $\text{m s}^{-2}$  for  $b$ , and  $\text{m s}^{-1}$  for  $w$ .

686

687

688

689



690

691

692 **Figure 5.** Vertical cross section of  $u$  from the second test case. A-2 is the analytical

693 solution. INC-2 is the numerical simulation with inhomogeneous Neumann condition for

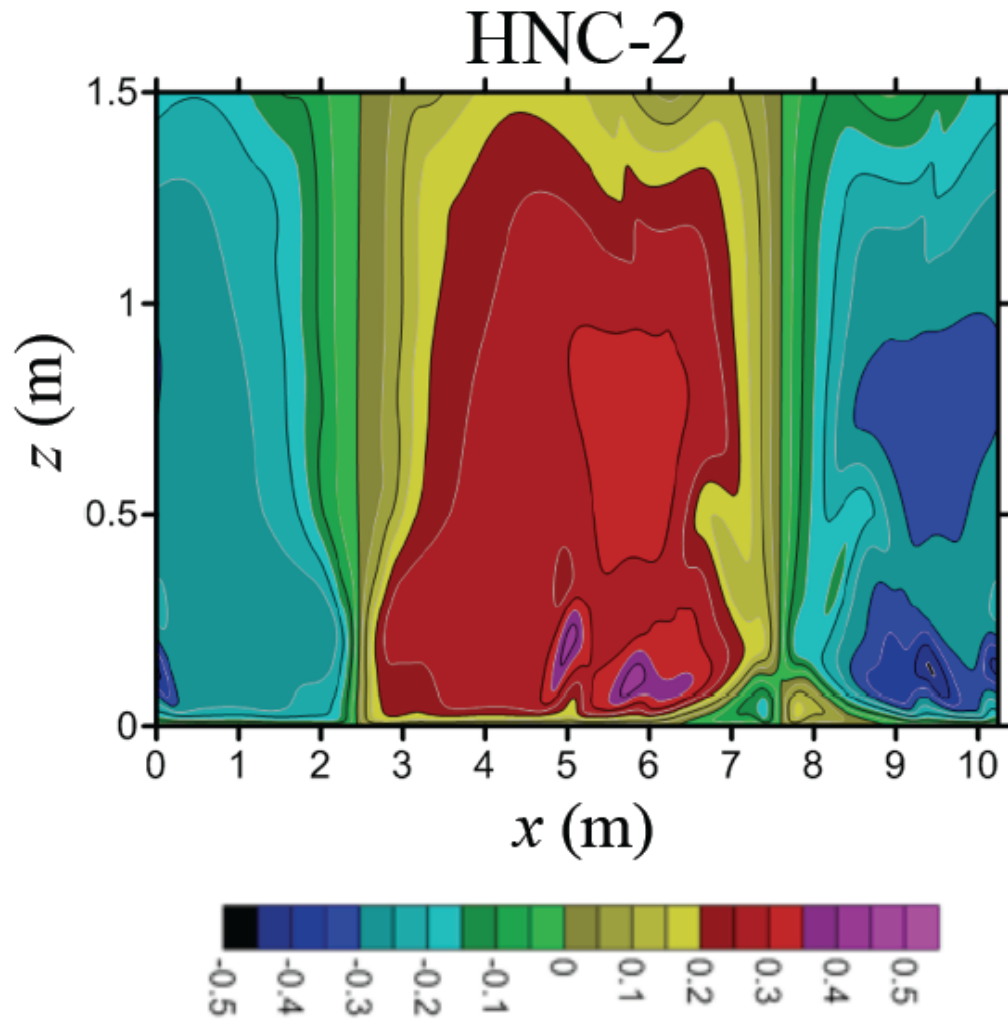
694 pressure. Color bar units are  $\text{m s}^{-1}$ .

695



696

697



698

699

700 **Figure 6.** Vertical cross section of  $u$  from HNC-2, the numerical simulation with

701 homogeneous Neumann condition for pressure in the second test case. Color bar units

702 are  $\text{m s}^{-1}$ .